Second-harmonic generation in doubly resonant microcavities with periodic dielectric mirrors

Marco Liscidini and Lucio Claudio Andreani
Dipartimento di Fisica "A. Volta," Università di Pavia, via Bassi 6, 27100 Pavia, Italy
(Received 26 July 2005; published 24 January 2006)

Strong enhancement of second-harmonic generation (SHG) is expected in one-dimensional microcavities when double resonance for the pump and the harmonic fields, as well as phase matching, are achieved. The realization of a doubly resonant microcavity with dielectric mirrors made of nonbirefringent materials is difficult because of the refractive index dispersion of the constituent media. Here we present a powerful method, based on photonic crystal concepts like gap maps and their generalization to defect modes, for the design of doubly resonant microcavities with periodic dielectric mirrors. The material dispersion is compensated by using the angle of incidence as a tuning parameter, thanks to the polarization splitting of cavity modes. The cavity enhancement of SHG increases exponentially with the number of periods in the dielectric mirrors and can be much larger than in single-resonant microcavities with comparable (or even larger) quality factors. The roles of phase delay and of thin versus thick configurations in the dielectric mirrors, of the growth orientation, and of the polarization degrees of freedom in achieving double resonance with phase matching are discussed. Significant examples of doubly resonant SHG with high conversion efficiency are given for $Al_{0.25}Ga_{0.75}As$ cavities with $Al_{0.4}Ga_{0.6}As$/Alox (oxidized AlAs) mirrors.

DOI: 10.1103/PhysRevE.73.016613 PACS number(s): 42.70.Qs, 78.20.Bh, 78.67.Pt, 42.65.Ky

I. INTRODUCTION

Since the first studies on second-harmonic generation (SHG), periodic structures have been indicated as a suitable solution for achieving phase matching even in cubic materials like GaAs, where there is no birefringence to compensate the refractive index dispersion [1,2]. Other forms of phase matching have also been proposed, like using form birefringence induced by refractive index modulation in the long-wavelength limit [3,4] or incorporating a separated quantum well region in the nonlinear media [5]. In the last few years the concept of photonic crystal has been increasingly applied to nonlinear optics [6,7], especially for what concerns frequency conversion. The possibility of tailoring the dispersion relation through a periodic modulation of the refractive index gives additional degrees of freedom to achieve phase matching, moreover using the high density of states at the band edges allows increasing the amount of pump power available in the nonlinear layers [8–13].

Another possible route for increasing SHG is to embed the nonlinear source in a Fabry-Pérot cavity, in order to enhance the pump field intensity or to optimize the extraction efficiency of the harmonic field. Several studies have been conducted on external cavities [14,15], where it is relatively easy to achieve double resonance for both the pump and harmonic frequencies. Concerning monolithic cavities with dielectric mirrors, most studies focused on SHG in the presence of a single resonance [16,17]. A doubly resonant microcavity is desirable since the performance of the structure can be optimized at both pump and harmonic frequencies. This problem has been discussed by Berger [18] who provides an analytic expression of the cavity enhancement of SHG for a doubly resonant monolithic cavity in the undepleted pump limit. In that work the double-resonance problem is studied for the case of metallic and pseudo-metallic mirrors, and for the latter case the concept of dual-wavelength dielectric mirrors (DWDM) based on non-$\lambda/4$ periodic structures is applied [18]. Experimental realization of a doubly resonant $Al_{0.3}Ga_{0.7}As$/AlAs microcavity has been reported by Simonneau *et al.* [19] but with the use of a specially designed structure with nonperiodic mirrors.

Starting from a previous work [20], in this paper we provide a systematic analysis of double resonant microcavities (DRMs) with periodic dielectric mirrors, describing in detail the main issues in the design of such structures and evaluating their nonlinear conversion efficiency. The fundamental brick which is used in order to construct a DRM is a dual wavelength dielectric mirror (DWDM), which is a distributed Bragg reflector (DBR) characterized by two stop bands centered at the pump frequency and at the second harmonic. The design of such mirrors is strongly limited by the refractive index dispersion of the constituent materials. Starting by considering a one-dimensional photonic crystal (1DPC), which represents the infinite system corresponding to a finite DBR, we provide an efficient method for the design of a DWDM taking into account the material dispersion. Several examples are discussed in Sec. II. The design of a DRM can also be performed by working with a corresponding photonic crystal system, in which the microcavity is described by the insertion of a defect in the 1DPC and the cavity structure is repeated with a supercell periodicity. In Sec. III the linear properties of DRM made of a $Al_{0.25}Ga_{0.75}As$ layer embedded in $Al_{0.4}Ga_{0.6}As$/oxidized AlAs(Alox) dielectric mirrors are studied, with particular emphasis on the possibility of using the incident angle as a tuning parameter and to take advantage of the polarization splitting of the cavity resonances. In Sec. IV we present the nonlinear results for SHG in two microcavity structures, designed for operation in different polarization conditions, and the DRMs performance is compared with the one of a single resonant microcavity (SRM). We discuss also the issue of phase-matching versus antiphase matching in a DRM. In Sec. V the results and conclusions of this work are summarized.

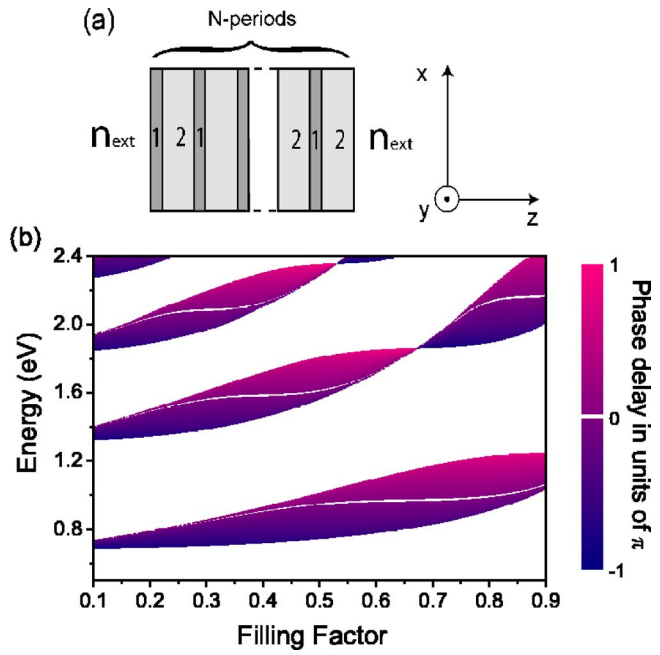

FIG. 1. (Color online) (a) Scheme of a distributed Bragg reflector. (b) Gap map as a function of the filling factor $f=L_1/(L_1+L_2)$, for a DBR consisting of Alox (material 1) and $Al_{0.4}Ga_{0.6}As$ (material 2) with period $\Lambda \equiv L_1+L_2=292$ nm. The reflection phase delay within the photonic gap is shown in color scale. All the calculations are performed assuming incidence angle $\theta=30°$ and p-polarized electric field.

The main advances with respect to our previous work [20] are as follows: (*i*) we consider $Al_{0.25}Ga_{0.75}As$ cavity layers and optimize the DRM structures for a pump wavelength $\lambda=1.55$ μm (instead of GaAs cavities for $\lambda=2$ μm); (*ii*) the design of a phase-matched DRM is made for a [001] growth orientation (instead of [111]); and (*iii*) a systematic discussion of the design strategy, of thick- and thin-DBR configurations, of the issue of phase-matching versus antiphase matching, and of the role of cavity Q factors is given here.

II. DUAL-WAVELENGTH DIELECTRIC MIRRORS

The possibility of designing a doubly resonant structure, in order to enhance the second-harmonic generation process, depends on the capability of growing dual-wavelength dielectric mirrors characterized by two stop bands, at the pump and harmonic frequencies. In this case one has to depart from the usual $\lambda/4$ condition, for which no stop band is present for the harmonic field, and look for a more general design. Different approaches are possible: optimizing the performances of the mirrors by building them layer-by-layer in a nonperiodic structure [19], or working with non-$\lambda/4$ periodic mirrors [18,20,21]. Here we assume to work only with periodic structures formed by the repetition of a bilayer period as sketched in Fig. 1(a). The equivalent infinite system is an ideal 1DPC, characterized by a periodic dielectric function along the z direction.

The solution of the Helmholtz equation for the electromagnetic field can be reduced to an eigenvalue problem, where the field is described by Bloch functions and the eigenvalues represent the energies allowed to the propagating modes. In perfect analogy with the electronic problem in a crystal, the eigenvalues can be organized in a photonic band structure [22]. The dispersion relations $\omega=\omega(k)$ for the propagating modes are found by the transfer-matrix method and Bloch-Floquet theorem in the form of an implicit equation that is the optical analog of the Kronig-Penney model [25]:

$$\cos(q\Lambda) = \cos(k_{1,z}L_1)\cos(k_{2,z}L_2) - \frac{1}{2}\left(\frac{\alpha_1}{\alpha_2}+\frac{\alpha_2}{\alpha_1}\right)\sin(k_{1,z}L_1)\sin(k_{2,z}L_2), \quad (1)$$

where $\Lambda=L_1+L_2$ is the DBR period, q is the Bloch vector, L_1 and L_2 are the layer widths [see Fig. 1(a)], $k_{i,z}=(\omega/c)n_i\cos\theta_i$, $i=1,2$, are the z components of the wave vectors in the layers, $n_i=n_i(\omega)$ are the refractive indices including material dispersion, while θ_i depends on the incident angle θ and the external refractive index n_{ext} through Snell's law $\theta_i=\arcsin[(n_{ext}/n_i)\sin\theta]$. Since we work at a finite incidence angle we have to distinguish between transverse electric (TE or s polarized) and transverse magnetic (TM or p polarized) modes, with the following expressions for the factors α_i of Eq. (1):

$$\left.\begin{aligned}\alpha_1 &= n_2\cos\theta_1\\ \alpha_2 &= n_1\cos\theta_2\end{aligned}\right\} \text{ TM modes,}$$

$$\left.\begin{aligned}\alpha_1 &= n_1\cos\theta_1\\ \alpha_2 &= n_2\cos\theta_2\end{aligned}\right\} \text{ TE modes.}$$

A notable feature of the formalism is that the material dispersion of the refractive indices can be easily taken into account. In the following examples we shall use the material dispersion of GaAs, AlAs, and Alox and of the $Al_xGa_{1-x}As$ alloy as reported in the literature [26].

As in the case of the Kronig-Penney model we find forbidden frequency intervals or *photonic gaps*, for which the Bloch vector is completely imaginary, corresponding to nonpropagating electromagnetic modes. Solving numerically Eq. (1) we can easily provide a map of the position of the gaps by varying the DBR parameters or the incidence angle. We show an example in Fig. 1(b), where the gap position of a DBR made of oxidized AlAs (or Alox, layer 1) and $Al_{0.4}Ga_{0.6}As$ (layer 2) is plotted as a function of the filling factor $f=L_1/\Lambda$ with $\Lambda=292$ nm, for an incidence angle $\theta=30°$ and p polarization. Notice that, when the $\lambda/4$ condition is fulfilled, the first-order gap has a maximum width while the second-order gap vanishes: the corresponding filling factor will be called $f\equiv f_{\lambda/4}$. Under this condition, the reflectance at the center of the first-order stop band is also maximum.

The gap maps available in the literature are usually reported in dimensionless units, since they are calculated for fixed values of the dielectric constant and they are scalable with the period of the photonic lattice [22]. Here the gap positions are reported in energy units because our goal is to

study the relative positions of the photonic gaps at ω and 2ω, hence the material dispersion cannot be neglected and the gap maps are not scalable.

Dielectric mirrors offer the advantage of great flexibility and the possibility of tuning the reflectance varying the number N of periods in the multilayer. A remarkable difference with respect to metallic mirrors is the phase change of the field associated to reflection. Indeed, while in a metallic mirror the phase of the field changes only of multiples of π, dielectric mirrors are characterized by a complex reflection coefficient

$$r = \sqrt{R}e^{i\phi}, \tag{2}$$

where $R=|r^2|$ is the mirror reflectance, while ϕ is the reflection phase which is, in general, a complicated function of the mirror structure, the external medium refractive index n_{ext}, and the field polarization and frequency.

In the case of periodic mirrors in the limit $R \simeq 1$ (i.e., for sufficiently large N), it has been demonstrated by Apfel [23,24] that the reflection phase delay within the stop bands depends only on the period composition and external medium refractive index but is independent of N. Moreover, the phase delays seen by two different external media, of refractive index n_0 and n_c, respectively, are related by the simple equation

$$n_0 \tan\frac{\phi_0}{2} = n_c \tan\frac{\phi_c}{2}. \tag{3}$$

In Fig. 1(b) we report an example of a map of reflection phase delay as a function of filling factor. The phase is shown in a color scale within the photonic gaps where, for the case of finite N, the reflectance is close to unity. The results for the phase delay in reflection will play a crucial role for the second-harmonic generation problem to be discussed in Sec. IV.

Let us look for a DWDM whose first-order gap (for the pump beam) is centered around the convenient wavelength $\lambda=1.55$ μm. In Figs. 2(a) and 2(b) we plot the gap maps for two systems with weak and strong refractive index contrast, respectively. The energies of the second-order gap (for the harmonic beam) are divided by 2 in order to visualize better the filling factors for which two gaps occur simultaneously at ω and 2ω: the darkest regions in the plots correspond to their superposition. In both cases we consider p-polarized pump, s-polarized second-harmonic beams and an angle of incidence $\theta=30°$.

Figure 2(a) refers to the case of AlAs/GaAs mirrors with $\Lambda=250$ nm. This material combination present a low refractive index contrast, therefore the photonic gaps are quite small, moreover the relatively high dispersion in the energy range under consideration makes the harmonic gap to lie below the pump one. The combination of these features allows designing a periodic DWDM only for a narrow range of filling factors $0.63<f<0.83$, with a very small superposition region in energy.

In Fig. 2(b) we present the case of a Alox/$Al_{0.4}Ga_{0.6}As$ DBR with $\Lambda=292$ nm. Now the harmonic gap is almost entirely contained in the pump one, hence a DWDM can be

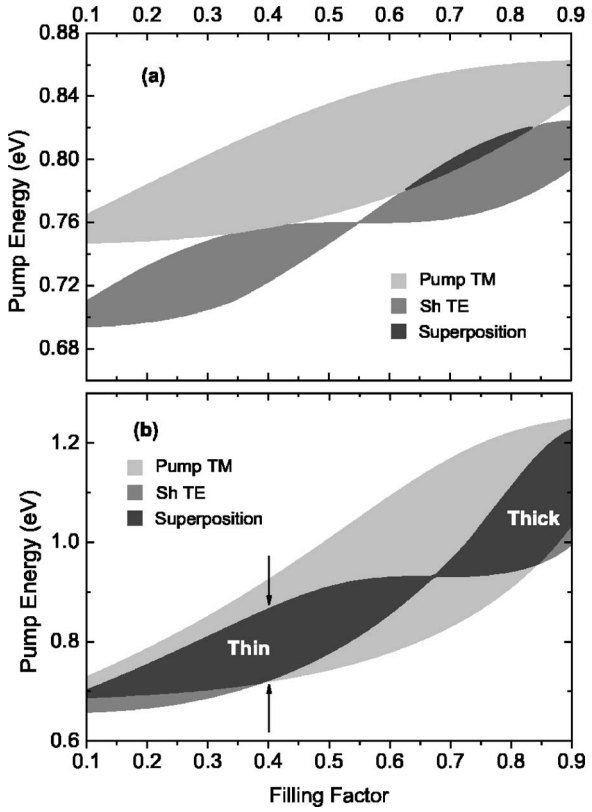

FIG. 2. Gap maps as a function of filling factor in a low index contrast AlAs/GaAs DBR with $\Lambda=250$ nm (a) and a high index contrast Alox/$Al_{0.4}Ga_{0.6}As$ DBR with $\Lambda=292$ nm (b). The energies of the harmonic gaps are divided by 2. In both cases we assume p-polarized pump, s-polarized harmonic, and an incidence angle $\theta=30°$.

realized for any filling-factor values, except the one corresponding to the $\lambda/4$ condition for which no harmonic gap occurs. With a filling factor $f=0.4$, which is the case indicated by arrows in Fig. 1(b), the pump gap is centered around 0.8 eV ($\lambda=1.55$ μm). The situation presented in Fig. 2(b) is the most advantageous one, indeed the small material dispersion guarantees that the pump and harmonic gap centers are close to each other for any filling factor values, while the high refractive index contrast allows us to achieve large gaps with a wide superposition region, and also to get high reflectance in the stop bands with a small number of DBR periods.

The solution presented in Fig. 2(b) for a Alox/$Al_{0.4}Ga_{0.6}As$ DWDM centered at 0.8 eV is not unique, since the period Λ or the incidence angle can be tuned in order to center the pump and harmonic gaps at the desired energy. The structures with a pump gap centered at 0.8 eV will be thinner when f is small, therefore we speak of a *thin configuration* when $f<f_{\lambda/4}$ and a *thick configuration* in the opposite case $f>f_{\lambda/4}$. It will be clear in Sec. IV that, in the case of a DRM, the choice of working in thin or thick configuration is not arbitrary. Indeed, as shown in Fig. 1(b), these two configurations are characterized by a different reflection phase: this fact has important consequences in the phase matching of the second-harmonic generation process.

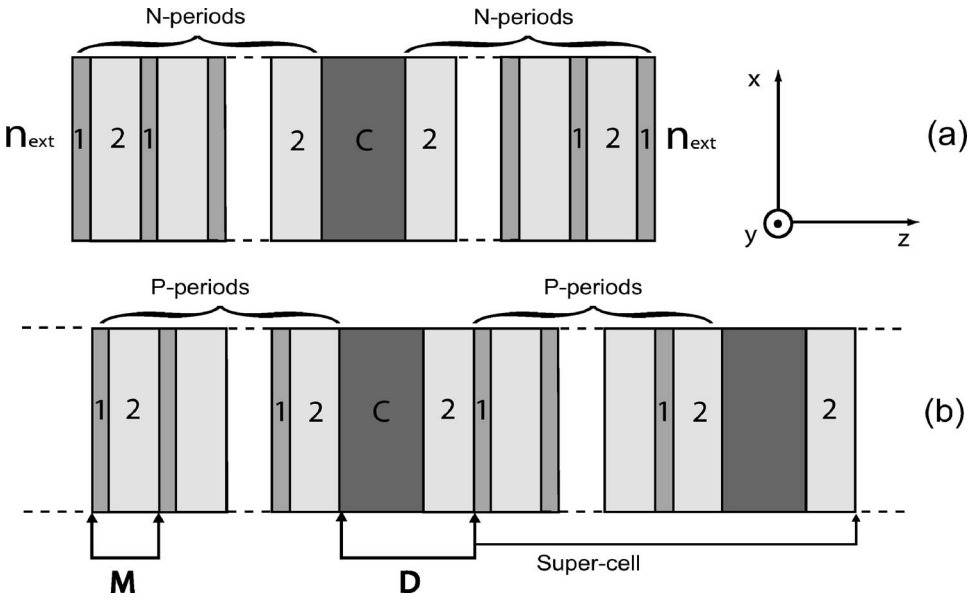

FIG. 3. Scheme of a doubly resonant microcavity (a) and the corresponding ideal periodic system (b).

Using the gap map technique it is possible to design a dual-wavelength dielectric mirror taking into account the refractive index dispersion. It has been shown that periodic DBR structures cannot be usefully employed in the case of low index contrast, highly dispersive material combinations like AlAs/GaAs. For these materials, nonperiodic structures like those of Ref. [19] may remain the best solution for the realization of dual-wavelength dielectric mirrors. In the more favorable case of high index contrast DBRs like $Alox/Al_{0.4}Ga_{0.6}As$, the superposition region between pump and harmonic gaps is sufficiently large to have a robust DWDM structure which can be tuned by changing either the DBR period (in the design) or the incidence angle (in the experiment). In the following section we discuss how such a DWDM can be used to achieve double resonance in a microcavity structure.

III. DOUBLY RESONANT MICROCAVITY

The possibility to obtain doubly resonant microcavities has been already investigated for pseudo-metallic mirrors at normal incidence [18] or for nonperiodic mirrors [19]. With metallic or pseudo-metallic mirrors the phase delay in reflection is $\phi=0$ or π and therefore the position of the resonances depends exclusively on the cavity length L_c. The index dispersion of the cavity material can be compensated by taking L_c to be equal to the coherence length [18]. Moreover, the temperature dependence of the refractive index is taken as an experimental tuning parameter. On the other hand, for nonperiodic dielectric mirrors, the cavity length is of the order of the wavelength of light and the angle of incidence is used as a tuning parameter [19]. The disadvantage of nonperiodic mirrors is that the structure is very sensitive to small deviations in the layer thicknesses, and also it is not easy to derive clear trends for the Q factors and the conversion efficiency as a function of structure length.

In this section we investigate the possibility of realizing a microcavity with two resonances centered at ω and 2ω, even in the presence of dispersive materials.

The idea is to employ periodic DWDM with high refractive index contrast and to use the angle of incidence as a fine-tuning parameter.

We consider a microcavity composed by a layer of width L_c embedded between two identical mirrors characterized by a complex reflection coefficient $r(\omega)=\sqrt{R(\omega)}\exp[i\phi(\omega)]$. The linear transmittance is

$$T(\omega) = \frac{(1-R(\omega))^2}{1+R(\omega)^2-2R(\omega)\cos\,\delta(\omega)} \tag{4}$$

with

$$\delta(\omega) = 2k_{c,z}(\omega)L_c + 2\phi(\omega), \tag{5}$$

where $k_{c,z}=(\omega/c)n_c\cos\,\theta_c$ is the z component of the wave vector, n_c is the refractive index in the cavity layer, and θ_c is found again by Snell's law. The system is resonant at specific frequencies ω_m when $\delta(\omega_m)$ is a multiple of 2π. The phase change $\phi(\omega)$ of a DBR is strongly dependent on frequency [23,24,27–30], thus the resonance position of the cavity mode inside the stop band is a complicated function of the structure parameters and of the incidence angle. Analytic expressions for the resonance position are available only when the cavity mode is close to the center of the stop band [29], where $\phi(\omega)$ can be approximated by a linear function of frequency.

Once a DWDM at the working frequency regions is designed (i.e., Λ, f, and θ are known), the DRM is obtained by introducing a defect with length L_c in the periodic structure, as shown in Fig. 3(a). We consider an equivalent infinite periodic system constituted by the repetition of a super-cell composed by $P+\frac{1}{2}$ periods of the DWDM and by the defect, as shown in Fig. 3(b). The presence of periodically repeated defects in the 1DPC structure introduces localized states in the photonic band gaps [31]. The problem of finding the desired cavity width for double resonance can be solved as follows. If we consider the transfer matrix $\mathbf{M}$ of a single

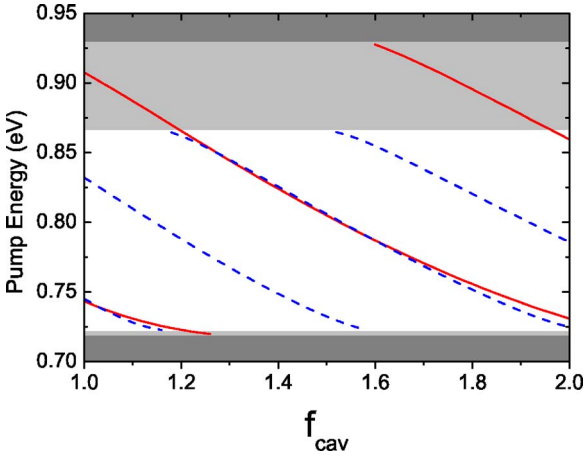

FIG. 4. (Color online) Position of p-polarized pump (solid lines) and s-polarized harmonic (dashed lines) defect modes inside their respective gaps as a function of $f_{\mathrm{cav}}=L_c/\Lambda$. The mirror is composed by $P=20$ periods of alternating $L_1=116.8$ nm (Alox) and $L_2=175.2$ nm ($Al_{0.4}Ga_{0.6}As$) layers, with $\Lambda=292$ nm; the incidence angle $\theta=30°$. Harmonic energies are divided by 2. The white region indicates an harmonic gap superimposed to the pump one (light gray), while the darkest zone indicates the absence of a gap.

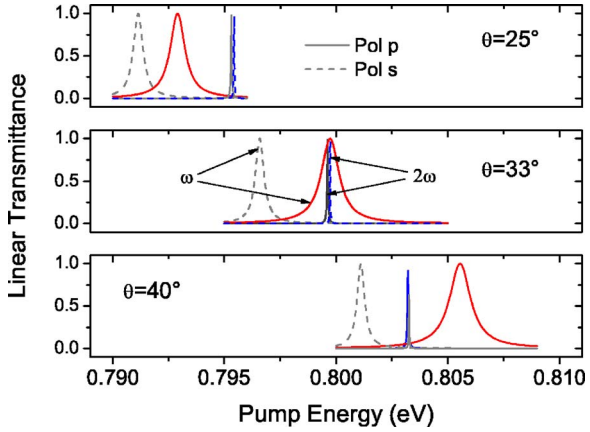

FIG. 5. (Color online) Tuning of the resonance positions by changing the incidence angle in a DRM: linear transmittance for p (solid) and s (dashed lines) polarizations for the pump and harmonic fields at $\theta=25°, 33°$, and 40°. Structure parameters: $L_1=116.8$ nm (Alox), $L_2=175.2$ nm ($Al_{0.4}Ga_{0.6}As$), and $L_c=449.7$ nm ($Al_{0.25}Ga_{0.75}As$), with $N=7$ periods in the DBRs. Double resonance occurs at $\theta=33°$.

mirror period and the transfer matrix $\mathbf{D}$ of the bilayer L_c/L_2 [see Fig. 3(b)], then the transfer matrix $\mathbf{T}$ of the super-cell is given by

$$\mathbf{T}=\mathbf{D}\mathbf{M}^P. \tag{6}$$

By indicating with $\mathbf{E_0}$ and $\mathbf{E}_{\Lambda_s}$ the electric field vector at the beginning and at the end of a single super-cell, discrete translational symmetry implies that

$$\mathbf{E}_{\Lambda_s}=e^{\imath q_s\Lambda_s}\mathbf{E_0}, \tag{7}$$

where $\Lambda_s=P\Lambda+L_2+L_c$ is the super-cell length and q_s is the Bloch vector. Thus it follows that $\exp(\pm\imath q_s\Lambda_s)$ are the eigenvalues of $\mathbf{T}$ and therefore

$$\mathrm{Tr}(\mathbf{T})=2\cos(q_s\Lambda_s). \tag{8}$$

This equation is the generalization of Eq. (1) and it contains implicitly the dispersion relation of the photonic system described above. In perfect analogy with the strategy we used in Sec. II, it is possible to provide a *defect map*, i.e., the positions of defect modes inside the gap can be evaluated as a function of the cavity length L_c or the incidence angle θ.

In Fig. 4 we show an example of a defect map, where the defect positions are plotted as a function of $f_{cav}=L_c/\Lambda$ [32]. As the thickness of the cavity layer increases, the defect modes move across the gap but with different slopes because of the material dispersion. For a wide range of f_{cav} values we find that the p-polarized defect mode is close to the s-polarized harmonic one. The small difference could be compensated by changing the angle of incidence. Here we choose the parameters in such a way that the double-resonance condition occurs close to the center of the stop bands, where the Q factor of the cavity modes is largest.

In the design of microcavity structures we chose to fulfill the double-resonance condition at a finite θ and for different polarizations of the pump and harmonic waves. In Fig. 5 we show the linear transmittance of a DRM for the pump and harmonic fields in both s and p polarizations. The harmonic energies were divided by 2 in order to visualize better the occurrence of a double resonance. Because of the polarization splitting of cavity modes, four resonances (two at ω and two at 2ω) are present. When the angle grows from $\theta=25°$ to $\theta=40°$, the resonances shift towards higher energies, and at $\theta=33°$ the p-polarized pump resonance overlaps the s-polarized harmonic one.

The power of the incidence angle as a tuning parameter depends on the strength of the polarization splitting [29,33]. A careful study of this problem, conducted through the defect-map method, has shown that the polarization splitting is extremely sensitive to the DBR parameters. In particular, the splitting is larger for a high refractive index contrast and when f is far from $f_{\lambda/4}$. In actual experiments, besides the incidence angle, the thickness variation of the epitaxial structure due to growth inhomogeneity could also be used to adjust the energy position of the double resonance.

As a general remark in closing this section, the gap- and defect-map methods represent an efficient tool for the design of microcavity structures. Moreover, this method can be applied even working at normal incidence when other resonance tuning parameters (e.g., temperature) can be used. Since the results are not scalable when material dispersion is considered, the design should be studied for each specific case. In the following we give examples of microcavities that are optimized for efficient SHG at double resonance.

IV. NONLINEAR RESULTS

In this section we analyze the results for second-harmonic generation (SHG) in a doubly resonant microcavity. Numerical calculations are performed using the nonlinear transfer matrix method [34] with the measured nonlinear susceptibili-

ties of the $Al_xGa_{1-x}As$ alloy [35] and are valid in the limit of negligible pump depletion. This assumption allows us to divide the SHG process in three independent steps: (*i*) linear propagation of the pump field, and (*ii*) generation of a nonlinear polarization and of a source field at the harmonic frequency, and (*iii*) propagation of the second-harmonic field along the structure. We show that in DRM all these aspects can be optimized simultaneously and a great enhancement of the nonlinear conversion can be achieved.

The second harmonic generated by the DRM can be compared to the one by the isolated cavity layer (or single-pass conversion). The ratio between the nonlinear transmittance of the cavity T_{cav}^{NL} and the one of the correspondent single layer T_{layer}^{NL} represents the enhancement due to the resonant cavity. Berger [18] has given an analytic expression for the cavity enhancement factor η of a symmetric structure:

$$\eta = \left| \frac{T_\omega \sqrt{T_{2\omega}} [1 + R_\omega \sqrt{R_{2\omega}} \exp(\imath \delta_{\mathrm{m}})]}{[1 - R_\omega \exp(\imath \delta_\omega)]^2 [1 - R_{2\omega} \exp(\imath \delta_{2\omega})]} \right|^2, \tag{9}$$

where $\delta_\omega = \delta(\omega)$ and $\delta_{2\omega} = \delta(2\omega)$ have been already specified in Eq. (5), while

$$\delta_{\mathrm{m}} = \phi_{j,\omega} + \phi_{k,\omega} + 2k_{z,\omega}L + \phi_{i,2\omega} + k_{z,2\omega}L, \tag{10}$$

where i,j,k are the Cartesian components coupled by the nonlinear susceptibility $\chi_{ijk}^{(2)}$. The factor δ_m describes the phase mismatch between the nonlinear polarization P^{NL} and the free harmonic field.

From Eq. (9) we observe that the cavity enhancement of SHG depends on the terms in curly brackets, which describe the effects of pump and harmonic field distributions (in the denominators) and of their phase mismatch (in the numerator). When a resonance at ω and 2ω occurs, the denominators of the expression (9) tend to vanish: this is the signature of a double-resonance condition. However, the SHG efficiency is enhanced only when the quantity $\delta_m \neq \pi[2\pi]$, otherwise the numerator also tends to vanish and the efficiency is reduced. The cavity enhancement is maximum when all the factors δ_ω, $\delta_{2\omega}$, and δ_m are multiples of 2π. Starting by the relations (5) and (10), it is easy to demonstrate that, in a *symmetric* cavity with double resonance, δ_m must be an integer multiple of π: the two situations that can occur are analyzed below.

When $\delta_m = 2n\pi$, which we call a *phase matching condition*, the nonlinear polarization is in phase with the harmonic field. For high reflectance mirrors we get

$$\eta_{\mathrm{pm}} \simeq \frac{4}{(1 - R_\omega)^2 (1 - R_{2\omega})} \propto Q_\omega^2 Q_{2\omega}. \tag{11}$$

In this situation all aspects of the harmonic generation process are optimized, and the cavity enhancement of SHG grows with the Q factors at ω and 2ω.

When $\delta_m = (2n+1)\pi$, which is called *antiphase matching condition*, the nonlinear polarization P^{NL} in the cavity layer is exactly out of phase with respect to the free harmonic field. This means that the coupling between the nonlinear polarization and the free harmonic field is weak, yielding a low extraction efficiency. Again we look at the $R_{\omega,2\omega} \to 1$ limit and obtain

$$\eta_{\mathrm{apm}} \simeq \frac{\left[1 - R_\omega + \frac{1}{2}(1 - R_{2\omega})\right]^2}{(1 - R_\omega)^2 (1 - R_{2\omega})}. \tag{12}$$

Here we observe that there are two types of behavior according to the rapidity with which R_ω and $R_{2\omega}$ tend to unit. In particular we obtain

$$\eta_{\mathrm{apm}} \simeq \frac{1 - R_{2\omega}}{4(1 - R_\omega)^2} \propto \frac{Q_\omega^2}{Q_{2\omega}} \tag{13}$$

when $(1-R_\omega)/(1-R_{2\omega}) \to 0$, and

$$\eta_{\mathrm{apm}} \simeq \frac{1}{(1 - R_{2\omega})} \propto Q_{2\omega} \tag{14}$$

when $(1-R_\omega)/(1-R_{2\omega}) \to \infty$ [36,37]. This result shows that, in the case of antiphase matching, the enhancement of SHG is much smaller than in the phase-matched situation.

The expressions (11), (13), and (14) can be compared with the enhancement factor of a single-resonant microcavity. We treat only the case of a resonance at the pump frequency ω. The cavity enhancement can be expressed as

$$\eta_{\mathrm{SRM}} = \frac{1}{(1 - R_\omega)^2} T_{2\omega} M_\omega \propto Q_\omega^2, \tag{15}$$

where $M(\omega)$ is a function describing the mismatch between the nonlinear polarization and the harmonic field. In general, since $T_{2\omega}$ and M do not present any resonance, pump field confinement is the only relevant effect.

The cavity enhancement factor is a function of mirror reflectance at ω and 2ω and therefore of the number N of periods in the DBRs. It is useful to express the Q factors as $Q \propto \exp(2N\kappa\Lambda)$, where κ is the imaginary part of the Bloch vector in the photonic gap. From expressions (11) and (13)–(15) we can derive the trend of the cavity enhancement as a function of N:

$$\eta_{\mathrm{DRM,pm}} \propto \exp[2N(2\kappa_\omega + \kappa_{2\omega})\Lambda], \tag{16}$$

$$\eta_{\mathrm{DRM,apm}} \propto \begin{cases} \exp[2N(2\kappa_\omega - \kappa_{2\omega})\Lambda], & \kappa_\omega \geqslant \kappa_{2\omega}, \\ \exp[2N(\kappa_{2\omega})\Lambda], & \kappa_\omega < \kappa_{2\omega}, \end{cases} \tag{17}$$

$$\eta_{\mathrm{SRM}} \propto \exp[4N\kappa_\omega], \tag{18}$$

The conversion efficiency η is largest in the phase matched DRM when

$$Q_{\omega,\mathrm{DRM}}^2 Q_{2\omega,\mathrm{DRM}} > Q_{\omega,\mathrm{SRM}}^2 \tag{19}$$

and the exponential growth with the number of period is faster when

$$2\kappa_\omega^{DRM} + \kappa_{2\omega}^{DRM} > 2\kappa_\omega^{SRM}. \tag{20}$$

This condition can be fulfilled by proper structure design, as illustrated below.

In expression (9) we have implicitly considered the case in which the generated second harmonic has a specific polarization and, in particular, that only one element $\chi_{ijk}^{(2)}$ of the

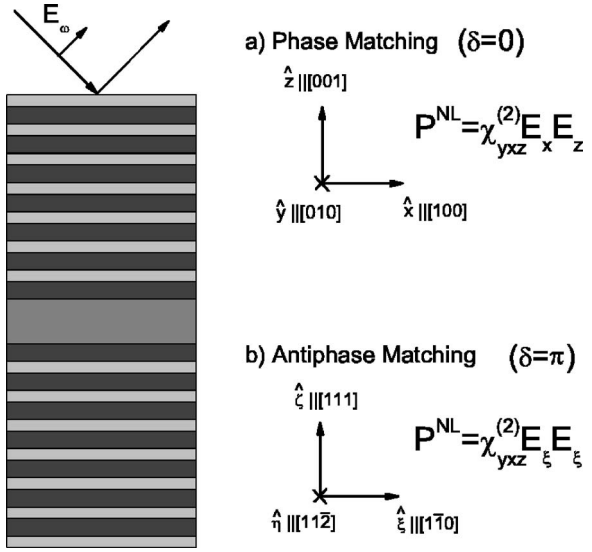

FIG. 6. Scheme of nonlinear microcavity, with two different growth directions [001] (a) and [111] (b). In the former case the nonlinear polarization is proportional to E_xE_z, while in the latter case P^{NL} is proportional to E_ξ^2.

nonlinear susceptibility is involved in the process. In general, for specific in/out polarization configurations, more than one tensor component is involved and the phase-matched one (if any) will be dominating. Also, Eq. (9) is derived by assuming that only the cavity layer be nonlinear. Thus Eq. (9) should be viewed as a useful guide for the design of microcavities with high SHG efficiency, but it cannot replace the numerical calculations to be presented below.

Although it is not possible to provide a general rule which tells *a priori* which DRMs are characterized by phase matching for a specific $\chi^{(2)}$ configuration, the DRMs can be divided in two classes, namely thick and thin, which depend on the DWDM used. We observe that, in general, these two classes are characterized by complementary behavior of δ_m. This fact is a consequence of the different phase delay which we have in thick and thin configurations at 2ω, in particular by looking at Fig. 1 we can notice that the phase delay changes by π when $f_{\lambda/4}$ is crossed. In our previous paper the design of a DRM was made in thick configuration [20], while in the present work a thin configuration is assumed. In the following we discuss examples of doubly resonant microcavities for *p-s* and *s-p* nonlinear conversion, respectively.

A. *p-s* configuration

The DRM is composed by a $Al_{0.25}Ga_{0.75}As$ cavity layer of width L_c=449.7 nm, embedded in two DWDM that are composed by alternated layers of Alox and $Al_{0.4}Ga_{0.6}As$, whose gap map is presented in Fig. 2(b). When f=0.4 we get a wide superposition of the pump and harmonic gaps around 0.8 eV, which corresponds to the following mirrors parameters: L_1=116.8 nm (Alox) and L_2=175.2 nm ($Al_{0.4}Ga_{0.6}As$). The pump resonance is tuned at the convenient wavelength of 1.55 μm (E=0.8 eV). This corresponds to the thin configuration marked with arrows in Fig. 2.

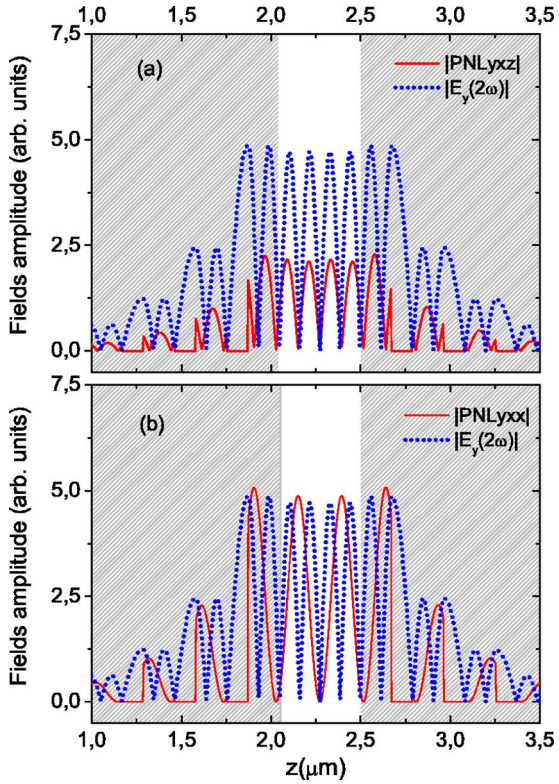

FIG. 7. (Color online) Nonlinear polarization (solid line) and free harmonic field (dashed line) in the DRM structure at the resonance frequency E=0.8 eV in the case of phase matching (a) and antiphase matching (b). The growth orientation is taken to be [001] and [111], respectively. The number of periods N=7 and the incidence angle θ=33°. The white area represents the cavity region.

The microcavity has been designed in order to achieve double resonance in *p-s* configuration and phase matching when the growth orientation is [001] so that the only relevant element of the nonlinear susceptibility tensor is $\chi^{(2)}_{yzx}$. In the case of a [001] growth direction [see Fig. 6(a)], the *s*-polarized nonlinear polarization is proportional to the product E_xE_z and, as it turns out, we get phase matching. In the opposite case of a [111] growth direction [Fig. 6(b)], instead, the nonlinear polarization is proportional to E_ξ^2. In this case the antiphase matching situation is realized.

If we look at the *s*-polarized nonlinear polarization and harmonic fields at the resonance frequencies, shown in Fig. 7, we notice that the two quantities oscillate in phase in the phase matching case (a) but are out of phase in the antiphase matching case (b). This figure allows us to visualize in physical terms the reason for the strongly increased SHG efficiency in the case of phase matching. However, these conditions are satisfied only inside the cavity layer. Since the $\chi^{(2)}$ of the $Al_{0.25}Ga_{0.75}As$ and $Al_{0.4}Ga_{0.6}As$ are comparable [35], the contributions of the nonlinear layers of the DWDM have to be considered. Nevertheless we observe that, in both cases, the behavior of the system is well described by Eq. (9): indeed at 0.8 eV the pump field is strongly confined in the cavity layer which represents the dominant contribution to harmonic generation.

Let us demonstrate more generally that the same structures parameters can be used in order to achieve double reso-

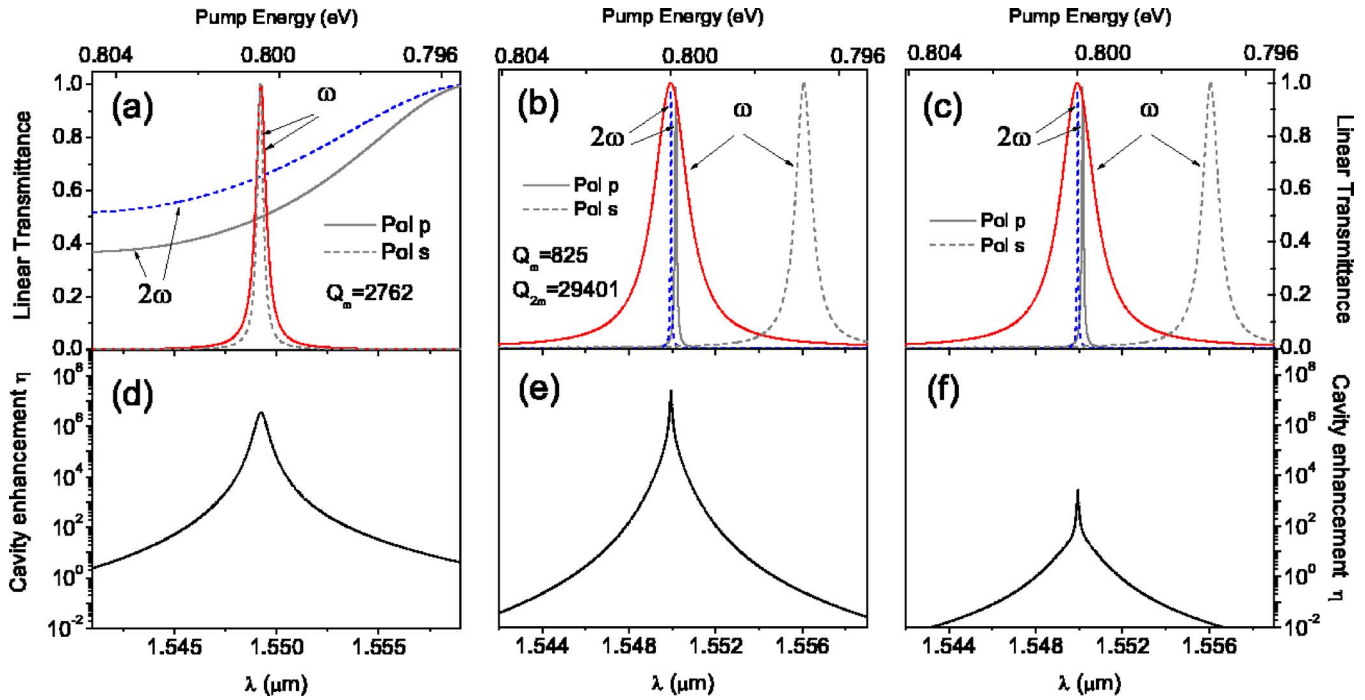

FIG. 8. (Color online) Linear transmittance versus pump wavelength for a single-resonant microcavity with [001] growth direction (a) and doubly resonant microcavities in the phase matching ([001] growth direction) (b) and antiphase matching ([111] growth direction) (c). The respective cavity enhancement factors are reported in panels (d),(e), and (f). The SRM and DRM are constituted by a cavity layer of $Al_{0.25}Ga_{0.75}As$ embedded in two mirrors composed by $N=7$ periods of alternating $Alox/Al_{0.4}Ga_{0.6}As$. In the case of SRM $L_c=242.8$ nm, $L_1=231.6$ nm, and $L_2=123.8$ nm, while for the DRM $L_c=449.7$ nm, $L_1=116.8$ nm, and $L_2=175.2$ nm. The pump and harmonic fields are p and s polarized, respectively. The incidence angle $\theta=29°$ for SRM and $\theta=33°$ for DRMs.

nance with phase- or antiphase matching when the growth direction is changed from [001] to [111]. From Eq. (10) we evaluate δ_m for the two different cases:

$$\delta_m^{[001]} = \phi_{x,\omega} + \phi_{z,\omega} + 2k_{z,\omega}L + \phi_{y,2\omega} + k_{z,2\omega}L, \quad (21)$$

$$\delta_m^{[111]} = \phi_{\xi,\omega} + \phi_{\xi,\omega} + 2k_{z,\omega}L + \phi_{\eta,2\omega} + k_{z,2\omega}L. \quad (22)$$

Since $\phi_{z,\omega}=\phi_{x,\omega}+\pi$, if we subtract (21) from (22) we obtain that

$$\delta_m^{[001]} - \delta_m^{[111]} = \pi. \quad (23)$$

Thus for the present p-s configuration it possible to switch from the phase-matching to the antiphase matching condition by changing the substrate orientation.

We compare the DRM with a single-resonant microcavity formed by a $\lambda/2$ layer of $Al_{0.25}Ga_{0.75}As$ with $L_c=242.8$ nm embedded between two identical $\lambda/4$ DBRs constituted by $N=7$ periods of $Alox/Al_{0.4}Ga_{0.6}As$ with $L_1=231.6$ nm, and $L_2=123.8$ nm. The linear transmittance at ω and 2ω and the cavity enhancement factor of the SRM and DRM in the phase matching and antiphase matching case are plotted in Fig. 8 as a function of pump wavelength. In the case of the SRM the pump linear transmittance exhibits two resonances tuned around 1.55 μm, while the transmittance at 2ω is structureless. Both DRMs are characterized by the same linear transmittance spectra, in particular we observe resonances for the p and s modes at ω and 2ω, double resonance being achieved in p-s configuration. From the linear spectra of Fig. 8 it is possible to have indication about the values of the Q factor for the pump and the harmonic resonances, in particular we notice that in the single-resonant microcavity Q_ω is greater than in the DRM. Nevertheless the cavity enhancement factor is about ten times larger in the DRM with phase matching because it is proportional to the product $Q_\omega^2 Q_{2\omega}$. Also, the DRM in phase-matching configuration has 10^4 higher SHG efficiency than in the antiphase matched case.

In Fig. 9(a) we compare the trends of the cavity enhancement factors calculated through the nonlinear transfer matrix method to the ones predicted by the analytical formulation as a function of the number N of mirror periods for the DRM. In all cases we observe an exponential growth. The phase-matched DRM exhibits the highest cavity enhancement for all values of N. For $N=6$ periods the enhancement factor is higher than 10^6. The analytical results are generally close to the numerical ones, except in the SRM, for which the mirror layers give a significant contribution and the analytic formula (9) underestimates the conversion efficiency.

In Fig. 9(b) we report the quality factors of the resonances involved in the nonlinear process. Note that, while the Q factors of the pump resonances are comparable, the Q factor of the harmonic one is considerably higher, therefore the cavity enhancement in the antiphase matching condition follows the trend predicted by Eq. (14). The higher Q factor at 2ω follows from choosing a p-s configuration (the DBR reflectance at finite angle of incidence is obviously higher for s than for p polarization). In real samples, the Q factors of

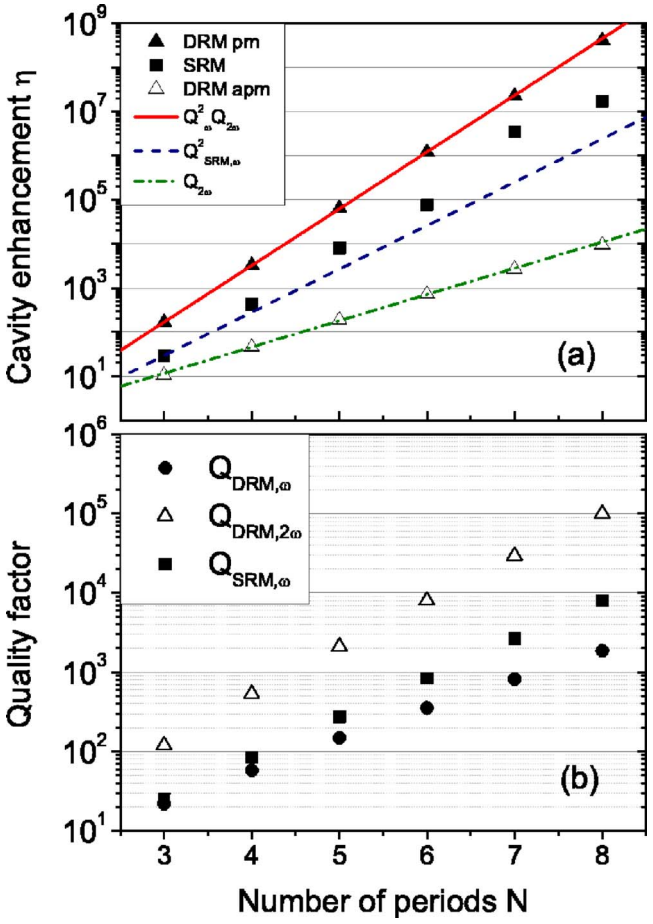

FIG. 9. (Color online) (a) Cavity enhancement factor in *p-s* configuration as a function of the number N of mirror periods for a double-resonant microcavity in phase matching and antiphase matching, and for a single-resonant microcavity. The symbols denote the results of the transfer matrix calculation, while the lines represent the exponential trend predicted by the analytical formulation. (b) Quality factors of the resonances at the pump and harmonic frequencies. Structure parameters are as in Fig. 8. The incidence angles are $\theta=29°$ and $\theta=33°$ for the SRM and DRM, respectively.

Fabry-Pérot in high-quality microcavities can be of the order of a few thousands: thus the enhancement factor for the present DRM is limited by the Q factor at 2ω. In the following subsection a different configuration with more balanced Q-factor values is proposed.

As compared to our previous work [20], the present structure has several novel features. First, the use of $Al_{0.25}Ga_{0.75}As$ (instead of GaAs) as a cavity layer allows designing a DRM for 1.55 μm pump wavelength. Second, working in the thin (instead of thick) configuration leads to a phase-matched structure for the more convenient [001] growth orientation. Finally, a DRM in thin configuration is always shorter than a thick DRM (or even a SRM) with the same number of periods and is therefore desirable when trying to minimize the device length.

B. *s-p* configuration

In this subsection we present a DRM with phase matching in which the Q factors at ω and 2ω are of the same order. We

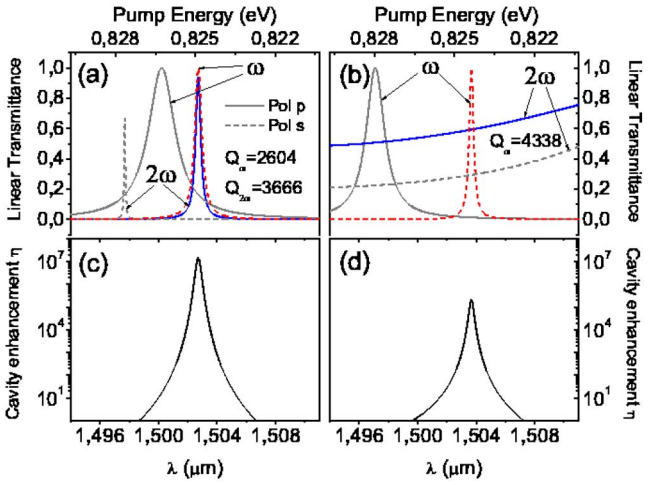

FIG. 10. (Color online) Linear transmittance versus pump wavelength for a phase-matched DRM (a) and a SRM (b) and their respective cavity enhancement factors in *s-p* configuration (c) and (d). The growth direction is assumed [001] and the incidence angle $\theta=41°$. The DRM and SRM are formed by a defect of $Al_{0.25}Ga_{0.75}As$ embedded in two mirrors composed by $N=5$ periods of alternating $Al_{0.4}Ga_{0.6}As$/Alox. In the case of DRM $L_c=744$ nm, $L_1=170$ nm, and $L_2=140$ nm, while for the SRM $L_c=245$ nm, $L_1=113$ nm, and $L_2=230$ nm.

choose to work in *s-p* configuration in order to reduce the Q factor at the harmonic frequency, while maintaining the polarization splitting of the cavity resonances in order to use the incidence angle as a tuning parameter. We consider only a [001] growth direction: in order to have a finite nonlinear polarization with *s*-polarized pump, the plane of incidence must be oriented along a [110] crystallographic axis. In other words, as compared to the structure shown in Fig. 6(a), the sample must be rotated by an azimuthal angle $\phi=45°$.

Following the gap-map method developed in Secs. II and III, we design a DRM in which double resonance is achieved for an incidence angle close to $\theta=40°$ at the pump wavelength $\lambda=1.5$ μm. We found the following parameters: the DRM is formed by a $Al_{0.25}Ga_{0.75}As$ layer of width $L_c=744$ nm embedded in $Al_{0.4}Ga_{0.6}As$/Alox DWDM with $L_1=170$ nm ($Al_{0.4}Ga_{0.6}As$) and $L_2=140$ nm (Alox). The SRM is made of a $\lambda/2$ $Al_{0.25}Ga_{0.75}As$ layer of width $L_c=245$ nm embedded between two $Al_{0.4}Ga_{0.6}As$/Alox $\lambda/4$ mirrors with $L_1=113$ nm($Al_{0.4}Ga_{0.6}As$) and $L_2=230$ nm (Alox). Note that the DBR layer nearest to the cavity is Alox, unlike in Sec. IV A.

In Fig. 10 the linear transmittance at ω and 2ω is plotted as a function of pump wavelength for the DRM (a) and the SRM (b) in *s-p* configuration. Again for the DRM we get a superposition of the pump and harmonic resonances, while in the SRM we have only one resonance centered around 1.5 μm for the *s*-polarized mode. It is interesting to observe that the Q factors of the DRM resonances are both lower than the SRM one. Nevertheless, the enhancement factor of the DRM is superior to that of the SRM by more than two orders of magnitude. Therefore in the present *s-p* configuration a DRM can have higher nonlinear conversion as compared to a SRM while requiring lower Q factors. Thus the

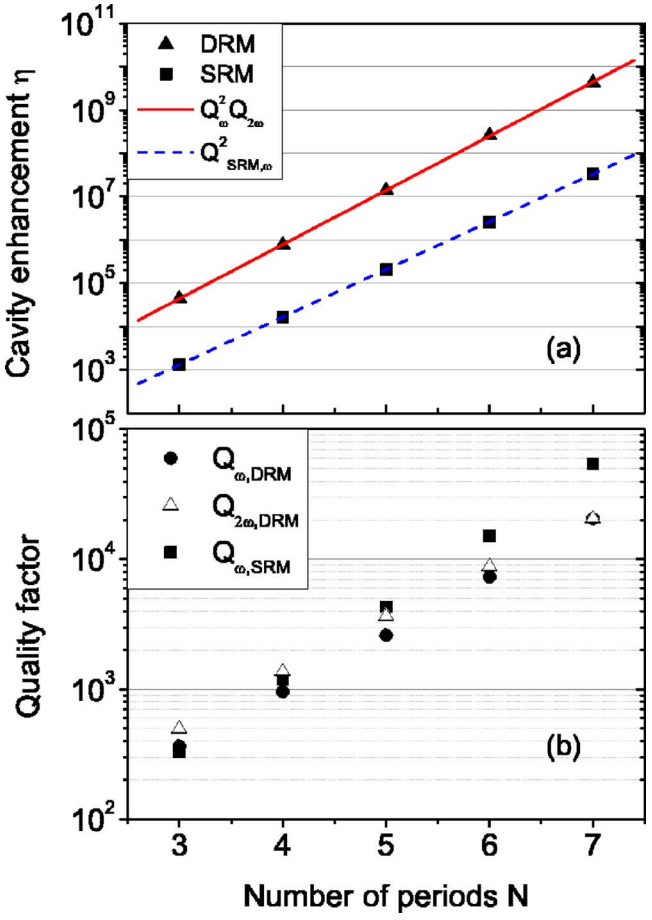

FIG. 11. (Color online) (a) Cavity enhancement factor in *s-p* configuration for a phase-matched double-resonant microcavity and for a single-resonant microcavity. The symbols denote the results of the transfer matrix calculation, while the lines represent the exponential trend predicted by the analytical formulation. (b) Quality factors of the resonances. Parameters are as in Fig. 10.

DRM is in all respects more convenient than a SRM.

In Fig. 11 we plot the cavity enhancement and the quality factors as a function of the number N of mirrors periods. Again the cavity enhancement η grows exponentially with N, moreover, there is good agreement between numerical and analytical calculations. This result follows from the different DBR configuration, in which the Alox layer is adjacent to the cavity one. In this way the index contrast close to the cavity increases; moreover, the two Alox layers do not present a $\chi^{(2)}$ nonlinearity, so that their contribution is vanishing.

The present DRM structure in *s-p* configuration allows achieving a cavity enhancement of the order of 10^7 with a device length smaller than 4 μm and Q factors of the order of a few thousands. The notable feature of this configuration is that the Q factors at ω and 2ω are comparable. Thus the present structure may be a convenient one in view of obtaining high nonlinear conversion in a double-resonant cavity system.

V. CONCLUSIONS

We have shown that it is possible to design doubly resonant microcavities using cubic materials where there is no birefringence to compensate the refractive index dispersion. To this purpose it is essential to realize dual-wavelength dielectric mirrors with two stop bands centered around the pump and the second-harmonic frequencies. The use of periodic mirrors allows the design to be carried out by means of the photonic gap map concept and makes the sample growth more robust against imperfections. Analogously, a planar microcavity can be viewed as a one-dimensional photonic crystal with a repeated defect layer. All the structure parameters can be found as a function of incidence angle and field polarizations. In this way the incidence angle can be used as a powerful experimental parameter in order to tune the relative pump and harmonic resonance positions, in particular by exploiting the polarization splitting in *p-s* and *s-p* configurations. The use of the angle of incidence as a tuning parameter can be very useful from an experimental point of view in order to compensate for possible growth inhomogeneities.

The symmetric doubly resonant microcavity is characterized by the presence of a precise phase relation between the nonlinear polarization and the harmonic field within the cavity layer. In particular we observe two different situations, namely phase matching and antiphase matching. In the phase-matched case the nonlinear polarization is perfectly in phase with the harmonic field, resulting in a very high cavity enhancement factor which can be more than two orders of magnitude greater than in an equivalent single resonant microcavity. Furthermore, the increase in nonlinear conversion can be achieved with Q factors at the pump and harmonic frequencies which are lower than in the reference single-resonant microcavity with $\lambda/4$ mirrors, therefore being less sensitive to growth imperfections. The conversion efficiency has been presented in terms of a cavity enhancement factor: according to the pump power level one may be able to reach the interesting (and potentially useful) situation in which the SH intensity is an appreciable fraction of the pump intensity. In this case, however, pump depletion effects can no longer be neglected and a more general treatment of the nonlinear conversion for the already optimized structure should be given. In the antiphase matched situation, the second-harmonic generation turns out to be much less efficient since the nonlinear polarization is out of phase with respect to the harmonic field and the extraction efficiency of the generated harmonic field is drastically reduced. In all these cases there is exponential growth of the conversion efficiency as a function of the number of periods in the dielectric mirrors. Specific design for phase-matched, doubly resonant microcavities in both *p-s* and *s-p* configurations have been provided that are amenable to experimental verification.

ACKNOWLEDGMENTS

The authors are grateful to M. Centini, A. Levenson, M. Patrini, and C. Sibilia for several discussions and valuable suggestions. This work was supported by MIUR through FIRB project "Miniaturized electron and photon system" and by INFM through PRA PHOTONIC.

[1] N. Bloembergen and A. J. Sievers, Appl. Phys. Lett. **17**, 483 (1970).
[2] J. P. van der Ziel and M. Ilegems, Appl. Phys. Lett. **29**, 200 (1976).
[3] A. Fiore, E. Rosencher, V. Berger, and J. Nagle, Appl. Phys. Lett. **67**, 3765 (1995).
[4] A. Fiore, V. Berger, E. Rosencher, P. Bravetti, and J. Nagle, Nature (London) **391**, 463 (1998).
[5] K. L. Vodopyanov, K. O'Neill, G. B. Serapiglia, C. C. Phillips, M. Hopkinson, I. Vurgaftman, and J. R. Meyer, Appl. Phys. Lett. **72**, 2654 (1998).
[6] See papers in *Nonlinear Optics of Photonic Crystals*, edited by C. M. Bowden and A. M. Zheltikov, feature issue, J. Opt. Soc. Am. B **19**, 1961 (2002).
[7] *Nonlinear Photonic Crystals*, edited by R. E. Slusher and B. J. Eggleton, Springer Series in Photonics, Vol. 10 (Springer, Berlin, 2003).
[8] M. Centini, C. Sibilia, M. Scalora, G. D'Aguanno, M. Bertolotti, M. J. Bloemer, C. M. Bowden, and I. Nefedov, Phys. Rev. E **60**, 4891 (1999).
[9] Y. Dumeige, P. Vidakovic, S. Sauvage, I. Sagnes, J. A. Levenson, C. Sibilia, M. Centini, G. D'Aguanno, and M. Scalora, Appl. Phys. Lett. **78**, 3021 (2001).
[10] G. D. Aguanno, M. Centini, M. Scalora, C. Sibilia, Y. Dumeige, P. Vidakovic, J. A. Levenson, M. J. Bloemer, C. M. Bowden, J. W. Haus, and M. Bertolotti, Phys. Rev. E **64**, 016609 (2001).
[11] G. D'Aguanno, M. Centini, M. Scalora, C. Sibilia, M. Bertolotti, M. J. Bloemer, and C. M. Bowden, J. Opt. Soc. Am. B **19**, 2111 (2002).
[12] Y. Dumeige, I. Sagnes, P. Monnier, P. Vidakovic, I. Abram, C. Mériadec, and A. Levenson, Phys. Rev. Lett. **89**, 043901 (2002).
[13] M. Centini, G. D'Aguanno, L. Sciscione, C. Sibilia, M. Bertolotti, M. Scalora, and M. J. Bloemer, Opt. Lett. **29**, 1924 (2004).
[14] A. Ashkin and G. D. Boyd, IEEE J. Quantum Electron. **QE-2**, 109 (1966).
[15] Z. Y. Ou and H. J. Kimble, Opt. Lett. **18**, 1053 (1993).
[16] T. V. Dolgova, A. I. Maidikovskii, M. G. Martem'yanov, G. Marovsky, G. Mattei, D. Schuhmacher, V. A. Yakovlev, A. A. Fedyanin, and O. A. Aktsipetrov, JETP Lett. **73**, 6 (2001).
[17] V. Pellegrini, R. Colombelli, I. Carusotto, F. Beltram, S. Rubini, R. Lantier, A. Franciosi, C. Vinegoni, and L. Pavesi, Appl. Phys. Lett. **74**, 1945 (1999).
[18] V. Berger, J. Opt. Soc. Am. B **14**, 1351 (1997).
[19] C. Simonneau, J. P. Debray, J. C. Harmand, P. Vidakovic, D. J. Lovering, and J. A. Levenson, Opt. Lett. **22**, 1775 (1997).
[20] M. Liscidini and L. C. Andreani, Appl. Phys. Lett. **85**, 1883 (2004).
[21] F. F. Ren, R. Li, C. Cheng, H. T. Wang, J. Qiu, J. Si, and K. Hirao, Phys. Rev. B **70**, 245109 (2004).
[22] J. D. Joannopoulos, R. D. Meade, and J. N. Winn, *Photonic Crystals* (Princeton University Press, Princeton, 1995).
[23] J. H. Apfel, Appl. Opt. **20**, 1024 (1981).
[24] J. H. Apfel, Appl. Opt. **21**, 733 (1982).
[25] P. Yeh and A. Yariv, *Optical Waves in Crystals* (Wiley, New York, 1984).
[26] *Handbook of Optical Constants of Solids II*, edited by E. D. Palik (Academic, Orlando, FL, 1991).
[27] H. A. McLeod, *Thin-Film Optical Filters*, 2nd ed. (Hilger, London, 1986).
[28] D. I. Babic and S. W. Corzine, IEEE J. Quantum Electron. **28**, 415 (1992).
[29] G. Panzarini, L. C. Andreani, A. Armitage, D. Baxter, M. S. Skolnick, V. N. Astratov, J. S. Roberts, Alexey V. Kavokin, M. R. Vladimirova, and M. A. Kaliteevski, Phys. Rev. B **59**, 5082 (1999); Phys. Solid State **41**, 1223 (1999).
[30] M. Galli, D. Bajoni, F. Marabelli, L. C. Andreani, L. Pavesi, and G. Pucker, Phys. Rev. B **69**, 115107 (2004).
[31] The number P of periods in the equivalent infinite systems should be enough large enough to avoid coupling between the different defects.
[32] R. P. Stanley, R. Houdré, U. Oesterle, M. Ilegems, and C. Weisbuch, Phys. Rev. A **48**, 2246 (1993).
[33] A. A. Dukin, N. A. Feoktistov, V. G. Golubev, A. V. Medvedev, A. B. Pevtsov, and A. V. Sel'kin, Phys. Rev. E **67**, 046602 (2003).
[34] D. S. Bethune, J. Opt. Soc. Am. B **6**, 910 (1989).
[35] M. Ohashi, T. Kondo, R. Ito, S. Fukatsu, Y. Shiraki, K. Kumata, and S. S. Kano, J. Appl. Phys. **74**,596 (1993).
[36] In Ref. [20] the limiting case of Eq. (13) was assumed.
[37] A. R. Cowan and J. F. Young, Phys. Rev. B **65**, 085106 (2002).